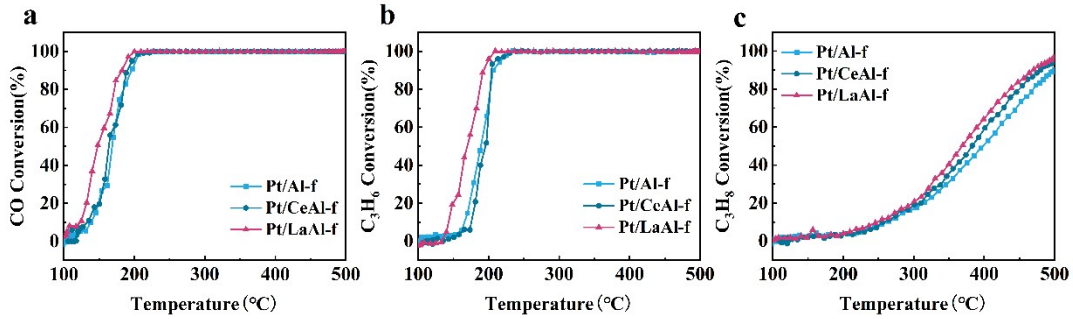

Figure S.1 Activity of Fresh Pt-Based Catalysts Supported by Different Carriers: a) CO Oxidation Activity Test; b) C_3H_6 Oxidation Activity Test; c) C_3H_8 Oxidation Activity Test.

Table S.1 Activity Data of Fresh Pt-Based Catalysts Supported by Different Carriers.

Sample	NO	CO		C_3H_6		C_3H_8	
	Max NO_2 proportion（%）	T_{50}(℃)	T_{90}(℃)	T_{50}(℃)	T_{90}(℃)	T_{50}(℃)	T_{90}(℃)
Pt/Al-f	79.2	168.2	201.3	186.1	202.6	398.9	497.6
Pt/LaAl-f	78.7	152.3	181.4	170.3	191.2	367.5	472.6
Pt/CeAl-f	75.7	164.3	197.3	188.5	201.5	378.0	480.4

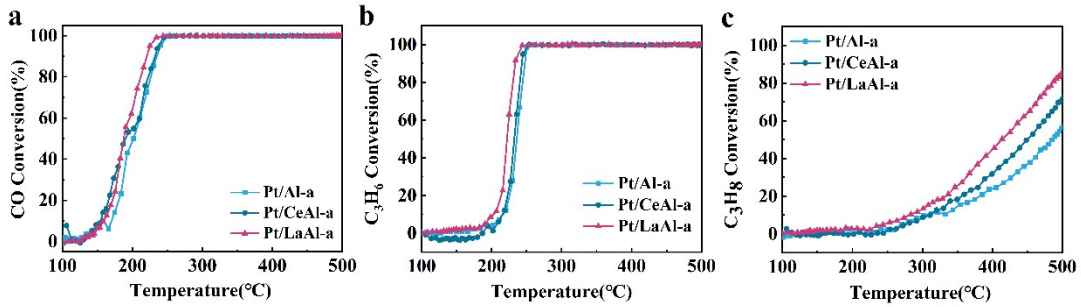

Figure S.2 Activity of Aged Pt-Based Catalysts Supported by Different Carriers: a) CO Oxidation Activity Test; b) C_3H_6 Oxidation Activity Test; c) C_3H_8 Oxidation Activity Test.

Table S.2 Activity Data of Aged Pt-Based Catalysts Supported by Different Carriers.

Sample	NO	CO		C_3H_6		C_3H_8	
	Max NO_2 proportion（%）	T_{50}(℃)	T_{90}(℃)	T_{50}(℃)	T_{90}(℃)	T_{50}(℃)	T_{90}(℃)
Pt/Al-a	59.5	206.6	233.0	239.1	248.5	581.3	-
Pt/LaAl-a	71.3	185.3	217.3	213.5	234.6	412.5	-
Pt/CeAl-a	60.0	197.3	232.4	236.4	245.5	448.9	-

Table S.3 Activity Temperature Windows of Pt-Based Catalysts Supported by Different Carriers.

Sample	NO		
	T_{in}(℃)	T_{out}(℃)	Temperature Window (℃)
Pt/Al-f	228.6	474.3	245.7
Pt/LaAl-f	205.3	476.3	271.0
Pt/CeAl-f	227.1	473.7	246.6
Pt/Al-a	259.6	476.7	217.1
Pt/LaAl-a	235.3	478.2	242.9
Pt/CeAl-a	254.9	477.1	222.2

Table S.4 Peak Information of Pt $4d_{5/2}$ for Fresh and Aged Pt-Based Catalysts Supported by Different Carriers.

Sample		Pt $4d_{5/2}$		
		B.E.（eV）	Peak(CPS • eV)	Pt^0 proportion（%）
Pt/Al-f	Pt^0	313.91	2045.82	71.31
	$Pt^{\sigma+}$	316.52	823.16	
Pt/LaAl-f	Pt^0	314.14	1388.60	75.36
	$Pt^{\sigma+}$	316.74	530.48	
Pt/CeAl-f	Pt^0	314.52	2557.65	72.74
	$Pt^{\sigma+}$	316.10	1659.89	
Pt/Al-a	Pt^0	314.33	1123.54	63.50
	$Pt^{\sigma+}$	317.31	645.76	
Pt/LaAl-a	Pt^0	313.87	3190.90	70.02
	$Pt^{\sigma+}$	316.90	1366.26	
Pt/CeAl-a	Pt^0	314.51	2569.18	60.64
	$Pt^{\sigma+}$	317.13	822.75	

Table S.5 Peak Information of O 1*s* for Fresh and Aged Pt-Based Catalysts Supported by Different Carriers.

Sample		O 1*s*		
		B.E.（eV）	Peak(CPS • eV)	O_{vac} proportion（%）
Pt/Al-f	O_{Lat}	531.00	331498.3	32.03
	O_{vac}	532.45	156244.1	
Pt/LaAl-f	O_{Lat}	531.14	301107.6	32.09
	O_{vac}	532.34	142287.5	
Pt/CeAl-f	O_{Lat}	533.15	413095.2	33.84
	O_{vac}	531.04	146607.1	
Pt/Al-a	O_{Lat}	532.35	398119.8	23.45
	O_{vac}	531.10	105955.5	
Pt/LaAl-a	O_{Lat}	532.38	316589.2	34.39
	O_{vac}	531.17	121934.5	
Pt/CeAl-a	O_{Lat}	531.49	110016.5	23.74
	O_{vac}	532.20	21599.4	

Table S.6 NO-TPD Data for Pt-Based Catalysts Supported by Different Carriers.

Sample	Adsorption integral area	Low-temperature desorption zone			High-temperature desorption zone		
		T(℃)	integral area S	Detachment rate（%）	T(℃)	integral area S	Detachment rate（%）
Pt/Al-f	15364.65	169	3332.36	21.69	376	3204.95	20.86
Pt/LaAl-f	19256.23	189	3390.69	17.61	386	4749.31	24.66
Pt/CeAl-f	16653.65	154	1564.81	9.40	355	4557.29	27.37
Pt/Al-a	12615.55	153	4331.77	34.34	406	6730.39	53.35
Pt/LaAl-a	17698.45	168	3746.97	21.17	402	10923.41	61.72
Pt/CeAl-a	10064.85	147	2295.36	22.81	354	6106.32	60.67

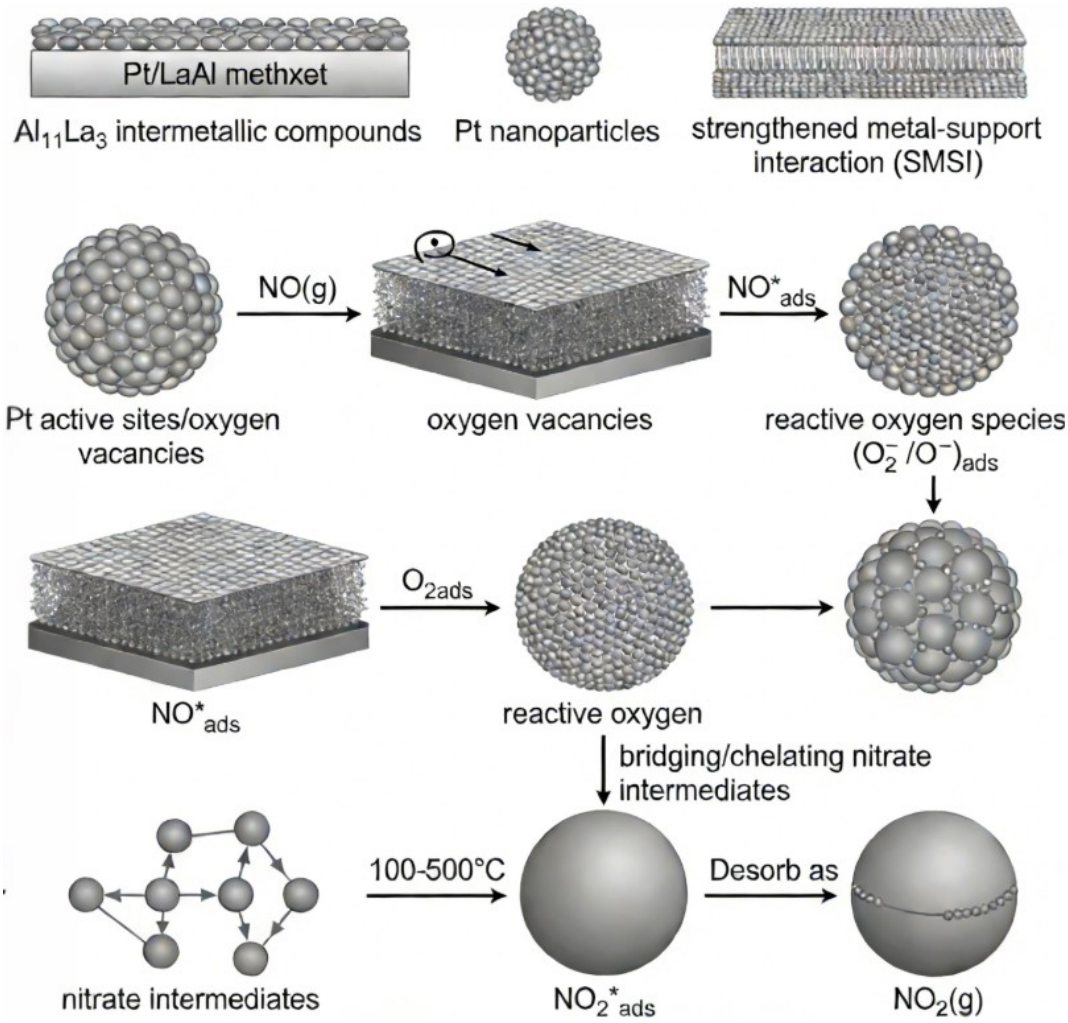

Figure S3. Schematic illustration of the NO oxidation reaction mechanism over the Pt/LaAl catalyst

La doping on γ-Al_2O_3 induces the formation of $Al_{11}La_3$ intermetallic compounds, which introduce additional Lewis acid sites and oxygen vacancies on the catalyst surface, while strengthening the metal-support interaction (SMSI) to effectively inhibit Pt nanoparticle aggregation and maintain high dispersion. Gaseous NO is adsorbed and activated on Pt active sites and oxygen vacancies to form NO_*ads, and O_2 is dissociated into reactive oxygen species (O_2^-/O^-)_ads at oxygen vacancies. The adsorbed NO*_ads reacts with reactive oxygen to form stable bridged/chelating nitrate intermediates, which are stabilized by the Lewis acid sites of $Al_{11}La_3$ to avoid premature desorption.

Finally, the stable NO_x* intermediates undergo thermal decomposition

at 100–500 °C to form NO_2*_ads, which desorbs from the catalyst surface as gaseous NO_2 product. The synergistic effect of $Al_{11}La_3$ and strengthened SMSI endows the catalyst with enhanced NO adsorption capacity, improved intermediate stability and excellent thermal aging resistance, thus leading to superior NO oxidation performance under simulated diesel exhaust conditions.